SYSTEM-ORIENTED MODELING AND SIMULATION OF BIOFLUIDIC LAB-ON-A-CHIP

Yi Wang[1], Ryan Magargle[2], Qiao Lin[1], James F. Hoburg[2], Tamal Mukherjee[2]
[1]Department of Mechanical Engineering, Carnegie Mellon University, U.S.A.
[2]Department of Electric and Computer Engineering, Carnegie Mellon University, U.S.A.
e-mail: yiw@andrew.cmu.edu

ABSTRACT

This paper presents a schematic-based and system-oriented modeling and simulation framework to enable top-down designs of multi-functional biofluidic lab-on-a-chip systems. An analog hardware description language (Verilog-A) is used to integrate parameterized and closed-form models of elements with different functionalities (e.g., mixing, reaction, injection and separation). Both DC and transient analysis are performed on a practical competitive immunoassay chip to capture the influence of topology, element sizes, material properties and operational parameters on the chip performance. Accuracy (relative error generally less than 5%) and speedup (>100×) of the schematic-based simulation is obtained by comparison to continuum numerical simulation as well as experimental measurements. A redesign of the original LoC device using our framework to improve bio-analysis efficiency and minimize chip-area has been demonstrated.

INTRODUCTION

While biofluidic lab-on-a-chip (LoC) systems have been widely studied in the past decade, their efficient simulation and design at the system-level continues to be a challenge. Experimental trial-and-error and numerical computation methods can lead to unacceptably long design cycles. Several modeling and simulation efforts have been proposed to speed up designs for specific subsystems [1-3]. However, no general methodology has been proposed to integrate these *element/component-level* models and enable the exploration of the entire *system-level* design space. To address this issue, this paper for the first time presents a system-oriented model for LoCs by linking previously developed element/component models [4-6]. The model accurately captures the effect of the chip topology, element size, material properties on chip performance. Therefore, our work represents a significant contribution to efficient modeling, simulation and designs of integrated LoCs.

SYSTEM-ORIENTED MODELING

Our system model is built on the geometric and functional hierarchy of the LoC. A multi-functional and integrated LoC generally consists of subsystems of different functionalities (Figure 1), which can be further decomposed into commonly used elements, such as straight mixing and turn separation channels. These elements are then modeled in a parameterized and closed-form manner, and stored in a VerilogA [4, 5] library. Connection pins are also proposed to interconnect them within the subsystem or among the different subsystems according to the spatial layout and physics. Therefore, by assembling element models users can quickly compose a complex system-oriented model/schematic for iterative-simulation based designs.

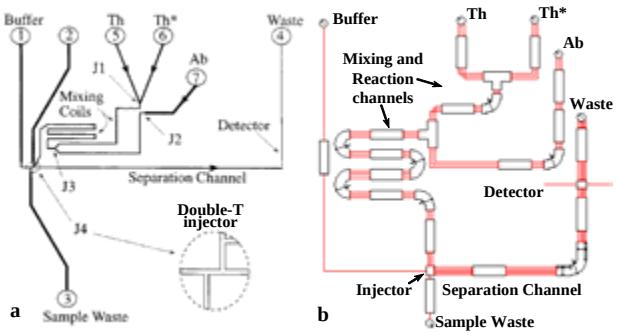

Figure 1. Sketch of a competitive immunoassay microchip [7] (a) and its system-oriented model/schematic (b).

In this paper, we will focus on the application of system-oriented modeling and simulation to a practical electrokinetic competitive immunoassay LoC [7], although the methodology can be readily extended to other biofluidic devices. Figure 1 illustrates the composition of such a LoC, which consists of four subsystems (mixing, reaction, injection and separation). Sample theophylline (Th, released from reservoir 5), first mixes with fluorescein-labeled theophylline tracer (Th*, released from 6) within channel J1-J3. Then the mixture competes for a limited number of antibody (Ab, released from reservoir 7) binding sites in the mixing and reaction channel J3-J4. The produced Ab-Th* complex and unreacted Th* (or called analyte hereafter) are injected into channel J4-Reservoir 4, where they are electrophoretically separated and detected. Therefore, the LoC operates in two phases: mixing-reaction-loading and dispensing-separation-detection [7]. The amount of Ab-Th* and Th*, represented by the areas under the electropherogram, for a wide range of Th concentration, can be post-processed to generate a calibration curve to determine unknown concentrations of sample Th for clinical analysis.

Pin Definition

In the system-oriented model, connection terminals of elements are represented by groups of pins. Each pin defines the state of biofluidic signal at the element terminal. Pins of adjacent elements are then linked by

0-7803-8952-2/05/$20.00

wires to enable signal transmission in the hierarchical LoC schematic. Therefore, pin definition affects both schematic composition and element modeling. There are two types of pins defined in the network. One is the electrical pin. This type of pin is independent of the functions achieved by the LoC and present in all elements, and used to construct a Kirchoffian network. Therefore, both the voltage at the pin and the current flowing through the element are captured. The second type of pin characterizes the biofluidic state (e.g., sample concentration and analyte band shape) at element terminals, which however is specific to the functions performed by the network.

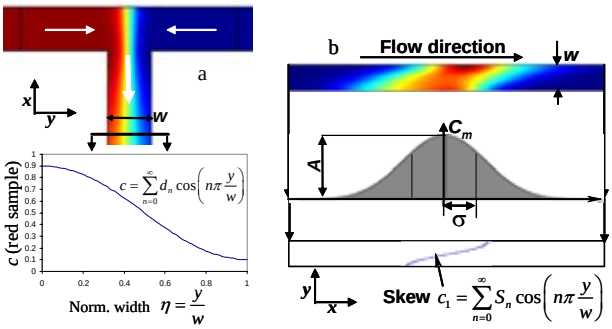

Figure 2. Biofluidic pin definition for a micromixer (a) and an electrophoretic separation microchip (b).

In this paper, various biofluidic pins are proposed to convey the states within or among the subsystems. For the micromixer, biofluidic pin is defined as a set of concentration coefficients $\{d_n\}$, the Fourier series coefficients of the sample concentration profile in the width direction and used to quantify the mixer performance (Figure 2a). The pins at the terminals of the separation element and detector, depicting the state of the analyte band shape, include variance (σ^2), the square of the standard deviation of the cross-sectional average analyte concentration (c_m) in the flow direction, measuring the width of the band; skew coefficients (S_n), used to describe the skew caused by turn channels; separation time (t), the moment the band centroid reaches the terminal; and amplitude (A), the maximum concentration (Figure 2b). The immunoassay reactor, bridging the mixer and injector, is modeled as a single element and hence owns different biofluidic pins at its inlet and outlet. At the inlet, it shares the same pin, the concentration coefficients $\{d_n\}$, as the mixer. At the outlet, average concentrations of reaction products (analyte) are provided to the downstream injector. The injector serves as the physical junction among reactor, separation subsystem and analyte-waste/buffer feeding channels, as well as the linkage between two operational phases. The shape (i.e., initial variance, skew coefficients and amplitude) of the injected analyte band is output by the injector outlet that is connected to the separation subsystem. The other two injector terminals leading to the feeding channels do not need biofluidic pins.

The values of biofluidic pins are calculated in terms of the directional signal flow. That is, their values at an element outlet are determined from the values at the inlet and the element's own contribution, starting from the most upstream element. The values are then assigned to those at the inlet of the next downstream element.

Element Models

The goal of each model is to obtain the input-output signal flow relationship of pin values at the inlet and outlet of each element. In addition, electrical resistance associated with each element relates the EK current flow through the element to the inlet and outlet voltages. As discussed above, the element models and the multi-physics captured by the models are different for individual biofluidic systems.

The micromixer library has nine element models, which are reservoirs (sample and waste), tapered straight channel, turns (90° or 180°, clockwise or counter-clockwise), diverging and converging intersections. Here, we will present the model for the mixing channel. Other elements can be modeled in a similar fashion [5]. Electrically, the tapered straight mixing channel is modeled as a resistor and the resistance is given by

$$R=\int_0^L \frac{dz}{w(z)h(z)C_e} \tag{1}$$

where w and h are the channel width and depth (functions of the coordinate z along the flow direction), C_e is the electric conductivity of the buffer in the channel. Then the concentration coefficients $d_n^{(in)}$ and $d_n^{(out)}$ at the inlet and outlet of the channel are related by [5]

$$d_n^{(out)}=d_n^{(in)}e^{-\gamma n^2\pi^2\tau} \tag{2}$$

where $\tau=LD/(\mu_{ek}E_{in}w_{in}^2)$, L is the channel length, w_{in} and E_{in} are the channel width and electric field at the channel inlet, D and μ_{ek} are the sample diffusivity and electrokinetic mobility, γ is a factor describing the effect of the channel cross-sectional shape on mixing [5].

The separation subsystem library includes nine basic models: turns (90° or 180°, clockwise or counter-clockwise), straight channel, feeding channel, reservoirs (sample and waste) and detector. Here the element model of the turn separation channel will be given to analyze the band-spreading (dispersion) effect due to turn geometry. Models of the other elements can be derived using the same principles [4]. Additionally, symbols and characters used in the following are defined the same as those for the mixer, unless otherwise noted. Electrically, the turn separation channel is also modeled as a resistor as shown in Eq. (1) with turn length L replaced by $L=r_c\theta$, where r_c and θ are the mean radius and angle included by the turn. The residence time Δt of an analyte band in the turn (the time for the band's centroid to move from the turn inlet to outlet) is given by

$$\Delta t=L/\mu_{ek}E \tag{3}$$

The changes in the separation time, skew coefficients and variance depend on Δt and are calculated by

$$t_{out} = t_{in} + \Delta t \tag{4}$$

$$S_n^{(out)} = \begin{cases} \pm \dfrac{8\theta w^2 \left(1 - e^{-(n\pi)^2 \Delta t D / w^2}\right)}{(n\pi)^4 \Delta t D} + S_n^{(in)} e^{-(n\pi)^2 \Delta t D / w^2} & , n \neq 0 \\ S_0^{(in)} & , n = 0 \end{cases} \tag{5}$$

$$\sigma_{out}^2 = \sigma_{in}^2 + 2D\Delta t \pm \frac{8w^4\theta}{D\Delta t} \sum_{n=1,3,5...}^{\infty} \left(\frac{S_n^{(in)} \left(1 - e^{-(n\pi)^2 D\Delta t / w^2}\right)}{(n\pi)^4} \right) + \frac{64 w^6 \theta^2}{(D\Delta t)^2} \sum_{n=1,3,5...}^{\infty} \frac{\left(-1 + e^{-(n\pi)^2 D\Delta t / w^2} + (n\pi)^2 D\Delta t / w^2\right)}{(n\pi)^8} \tag{6}$$

where subscripts/superscripts *in* and *out* represent quantities at the inlet and outlet of the turn. In Eqs. (5) and (6), the "+" sign is assigned to the first turn and any turn strengthening the skew caused by the first; the "-" sign is assigned to any turn undoing the skew from the first [4]. In addition, removing all the terms involving θ reduces to the special case for a straight separation channel. Assuming a Gaussian distribution of the average concentration c_m of the analyte band at element terminals always, we can obtain the amplitude by

$$A_{out} / A_{in} = \sqrt{\sigma_{in}^2 / \sigma_{out}^2} \tag{7}$$

A reactor model specific to the immunoassay reaction (Eq. (8)) in Figure 1 is also developed,

$$\begin{aligned} Th + Ab &\underset{k_2}{\overset{k_1}{\longleftrightarrow}} Ab - Th + Th \\ Th^* + Ab &\underset{k_4}{\overset{k_3}{\longleftrightarrow}} Ab - Th^* + Th^* \end{aligned} \tag{8}$$

According to Reference [7], we make several assumptions to simplify the modeling of Eq. (8): first, Th and Th* have the same binding affinity to Ab; second, the reaction is essentially irreversible, that is, $k_1 >> k_2$ and $k_3 >> k_4$; third, the reaction is mass-transport limited, hence mass transport and the binding process are decoupled and the latter is treated as instantaneous, with the prerequisite of complete mixing of Th, Th* and Ab at the reactor inlet. Based on these assumptions, the amount of Ab bound to Th and Th* is directly proportional to the molar concentrations of Th and Th*. A more generalized model that can handle reversible reaction kinetics and accommodate the incomplete sample mixing is in progress at authors' group.

The double-tee injector [7] is also modeled in terms of a single element using a functional modeling approach implemented with neural networks [6]. It takes the analyte concentrations (Th* and Ab-Th*) from the reactor as the input, as well as the calculated electrical fields in the leg channels at both phases, which shape and drive the injected analyte band [6]. Due to the transitional electric field at the injection intersection, the injected analyte band exhibits an irregular shape. However, for an efficient interface to the separation element models, the band output by the injector model is assumed to have an equivalent Gaussian distribution, which yields the same variance and analyte amount as the actual one [6]. Quantitative analysis (not shown here) indicates that this assumption holds very well for most biofluidic systems, including the LoC in Figure 1.

SYSTEM-ORIENTED SIMULATION

The system-oriented model/schematic including both wired pins and element models is illustrated in Figure 1b, which is simulated in two consecutive phases in consistence with its operation. At the first phase, loading voltage is applied between reservoirs 5, 6 7 and 3 with the others left floating. Then the electric field, concentrations of the sample, antibody and analytes in the mixer and reactor will be determined. At the double-tee injector, analyte concentrations and electric field in leg channels are saved. At the second phase, the potential is first set on reservoirs 1 and 4 with others left floating. The electric field is calculated and used to determine the band-shape of the injected analytes, along with the information saved in the first phase. This then initiates the simulation of the separation and detection subsystem.

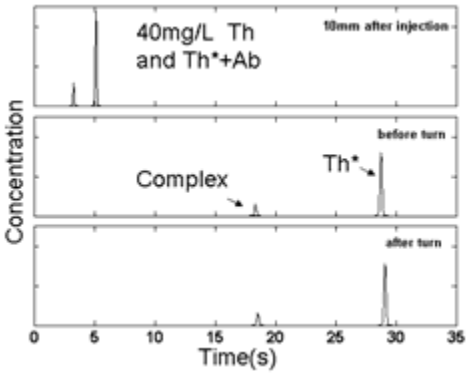

Figure 3. Electropherogram of Ab-Th* complex and unreacted Th* from system-oriented simulation.

Table 1. Comparison of height and area ratios among experiment [7], numerical simulation, and system modeling+.

	Experiment	Numerical	Sys. Simu
Area ratio Th*	~0.83	0.845	0.84
Area ratio Ab-Th*	~0.17	0.155	0.16
Peak height ratio	~5	4.98	5.0

+Actual concentrations for Th* is not available. Value was extracted from the results in [7].

Our simulation results are shown in Figures 3-5 and Table 1-2. Figure 3 shows the simulated electropherograms at three detection spots. It is observed that analyte bands of Th* and Ab-Th* complex gradually separate during their migration through the separation channel and the molecular diffusion is the major dispersion source in such a system. The height ratio and area ratio of the species bands are extracted at the third detector (Figure 3c) and compared with numerical simulation in Table 1; and very good agreement is obtained.

In Figure 4, a calibration curve of the area ratio for unreacted Th* and Ab-Th* complex is obtained from system simulation results by varying the concentrations

of Th sample. Very good agreement is found between the system simulation results and the numerical simulation as well as the experimental results (10% error). We can see that as the concentration of Th increases, more Ab will be bound to Th, leading to more unreacted Th* left in the analyte and the growth of Th* area ratio.

With the validation of our system-oriented model, we then take advantage of it to improve the original design (Figure 1a). Figure 5 shows the redesign by reducing the excessive mixing length and arranging it into a compact serpentine geometry. Additionally, the overly long separation channel is shortened, which hence increases the electric field and minimizes the band dispersion due to diffusion. Furthermore, the detector is also moved to the front of the 90° turn separation channel to avoid the turn-geometry induced dispersion at the high electric field in the new design. In Table 2, although the separation resolution drops to 15, it is still high enough to resolve the analyte bands (Figure 3). Most importantly, an impressive 1.6-fold increase in peak height and nearly 3-fold and 10-fold decrease in variance and chip area is achieved.

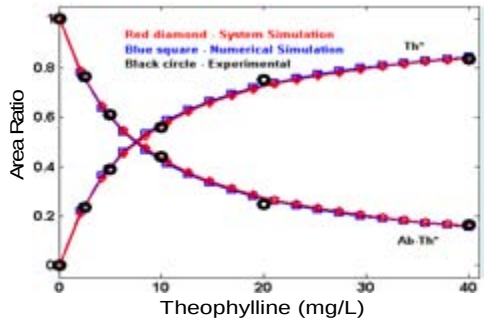

Figure 4. Comparison of the calibration curves from system modeling, numerical simulation and experimental data [7] for unreacted Th* and Ab-Th* complex vs the concentration of Th.

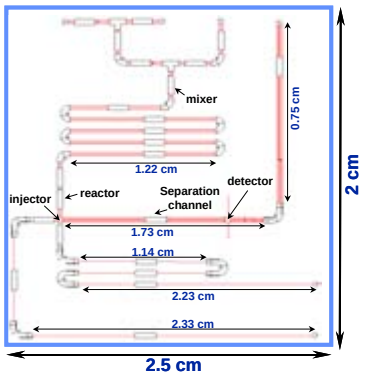

Figure 5. Schematic (not in scale) of the improved design of Figure 1a using the system-oriented model/schematic.

Table 2. Comparison of the separation time, variance, peak height and chip area between the original design and improved design.

Parameters	Original		Improved	
	Ab-Th*	Th*	Ab-Th*	Th*
Separation Time (s)	18.6	29.1	2.12	3.32
Variance (μm^2)	66607	30091	15654	11267
Peak height (norm.)	1	5	2	8.3
Resolution	24		15	
Chip area	7.6 cm × 7.6 cm		2.5 cm × 2 cm	

CONCLUSION

The methodology and applications of system-oriented modeling and simulation of an electrokinetic biofluidic lab-on-a-chip have been presented and demonstrated. The libraries of parameterized and closed-formed element models have been developed using an analog hardware description language (Verilog-A). Both electric and biofluidic pins are proposed to link the elements to form a system-level model/schematic, which allows for fast and iterative simulation and designs. DC and transient analyses of a practical competitive immunoassay LoC have been employed to capture the overall effects of chip topology, element size, material properties and operational parameters on the on-chip mixing, reaction, injection and separation. Our system simulation results have been verified by numerical and experimental data. An impressive speedup (>100) can be achieved over the numerical continuum simulation, while still maintaining high accuracy (relative error less than 5%). A design that improves analysis quality but occupies less chip-area has been demonstrated as well. Therefore, our modeling and simulation framework represents an effective and efficient CAD tool for system-level synthesis and optimal designs of electrokinetic lab-on-a-chip systems.

ACKNOWLEDGEMENT

This research is sponsored by the DARPA and the Air Force Research Laboratory, Air Force Material Command, USAF, under grant number F30602-01-2-0587, and the NSF ITR program under award number CCR-0325344.

References

[1] J. I. Molho, A. E. Herr, B. P. Mosier, J. G. Santiago, T. W. Kenny, R. A. Brennen, G. B. Gordon, and B. Mohammadi, "Optimization of turn geometries for microchip electrophoresis," *Anal. Chem.*, vol. 73, pp. 1350-1360, 2001.

[2] F. Schonfeld, K. S. Drese, S. Hardt, V. Hessel, and C. Hofmann, "Optimized distributive micro-mixing by 'chaotic' multilamination," *Proceedings of the Seventh International Conference on Modeling and Simulation of Microsystems (MSM'2004)*, pp. 378-381, Boston, MA, 2004.

[3] S. V. Ermakov, S. C. Jacobson, and J. M. Ramsey, "Computer simulations of electrokinetic injection techniques in microfluidic devices," *Anal. Chem.*, vol. 72, pp. 3512-3517, 2000.

[4] Y. Wang, Q. Lin, and T. Mukherjee, "System-oriented dispersion models of general-shaped electrophoresis microchannels," *Lab on a Chip*, vol. 4, pp. 453-463, 2004.

[5] Y. Wang, Q. Lin, and T. Mukherjee, "A model for complex electrokinetic passive micromixers," submitted to *Lab-on-a-chip*, 2005.

[6] R. Magargle, J. F. Hoburg, and T. Mukherjee, "Microfluidic injector models based on neural networks," *Proceedings of the Eighth International Conference on Modeling and Simulation of Microsystems (MSM2005)* (Accepted), 2005.

[7] N. H. Chiem and D. J. Harrison, "Microchip systems for immunoassay: an integrated immunoreactor with electrophoretic separation for serum theophylline determination," *Clinical Chemistry*, vol. 44, pp. 591-598, 1998.